Free Energy Calculation of Fluid-rock Interactions at Oil-shale Interface Using Molecular Dynamics Simulation

Zelong Zhang,*[,†] Haoran Liu, [‡,⊥] and Jianwei Wang[†,§]

[†]Department of Geology and Geophysics, Louisiana State University, Baton Rouge, LA 70803, United States

[‡]Department of Experimental Statistics, Louisiana State University, Baton Rouge, LA 70803, United States

[⊥]Department of Oceanography and Coastal Sciences, Louisiana State University, Baton Rouge, LA 70803, United States

[§]Center for Computation and Technology, Louisiana State University, Baton Rouge, LA 70803, United States

Corresponding to: zelongz@lsu.edu

Abstract

Understanding the fluid-rock interactions in shale nanopores is essential for the characterization of the transport and storage of hydrocarbon in oil reservoir rocks of tight formations such as shale. Due to the strong surface effect in nanospace and the heterogeneous nature of hydrocarbon systems, it is a great challenge to study the oil-shale interfaces. Molecular Dynamics simulations were applied to investigate the interaction of light oils with calcite and kerogen surfaces. Octane and octanthiol were used as model molecules to represent non-polar and polar oil compounds. A model molecule of kerogen fragment was implemented as the building block to construct kerogen surfaces which is the major constituent of shale organics. Calcite (104) surface was used due to its hydrophilic property of its surfaces and its ubiquitous presence in formation rocks, especially in carbonate shales. Umbrella Sampling method together with Weighted Histogram Analysis Method was employed to calculate the free energy profile of oil desorption on the surfaces of kerogen and calcite. The effects of oil polarity, size of oil molecular cluster, and water on the free energy were investigated. The results show that at molecular scale, the free energy of desorption of oil molecules is significantly reduced from both kerogen and calcite surfaces if water is presented. For polar oil molecule, the free energy of desorption is higher than that of non-polar oil at both calcite and kerogen surfaces. The organic kerogen surface exhibits stronger binding energies of oil molecules than the inorganic calcite. These findings suggest that 1) polar oil compounds require more effort to be recovered than non-polar ones, 2) oil clusters of a smaller size are harder to be displaced than a larger size, and 3) the presence of water decreases the free energy of desorption. This study provides energetic perspective of the interactions and insights on the oil recovery in shale formations. The methodology presented in this study demonstrates that MD simulation is capable to 1) evaluate the impact of different factors to the oil recovery in shale play and 2) offer valuable implications for developing novel technologies of oil recovery from unconventional shale.

41

TOC

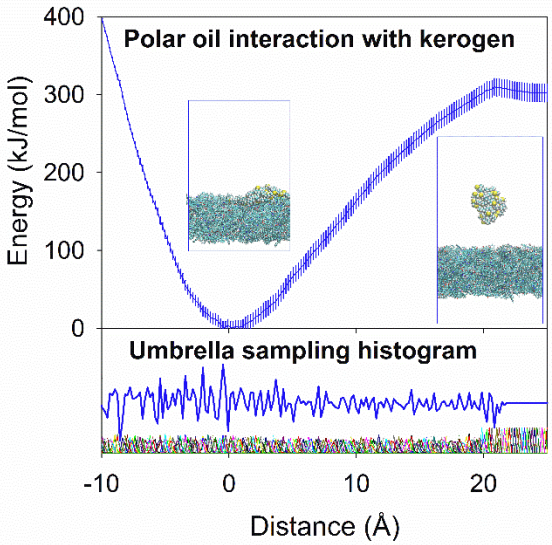
Polar oil interaction with kerogen
Umbrella sampling histogram
Energy (kJ/mol)
400
300
200
100
0
-10
0
10
20
Distance (Å)

42

1 Introduction

Ultra-tight formations, such as shale, bear abundant hydrocarbon fluid in poorly connected nanoscale pores with extremely low porosity and permeability.[1,2] The flow properties of transport and storage of fluid confined in nanopores deviates substantially from those of its bulk phase. This deviation is largely caused by the surface interactions within nanospace.[3–5] The interactions between the fluid and pore surface can affect a large portion of confined fluid molecules depending on the pore size and interfacial interactions, which leads to dramatic differences in the behaviors of fluid migration and storage in nanopores, compared to those of bulk phase fluid.[6,7] For instance, if the pore size decreases from 100 nm to 10 nm, the affected volume of the fluid increases from 17% to 100% by the intermolecular interactions with surface (assuming the affected radius is 3 nm) as shown in Fig 1. Significant amounts of hydrocarbon in ultra-tight reservoirs are confined in the nanopores,[8] mostly in organics and associated with minerals.[9,10] To understand how the hydrocarbon is stored in the formation rocks, it is vitally important to understand the interfacial interactions between the hydrocarbon fluid and nanopore surfaces in ultra-tight formation. Since oil recovery process is linked to the interfacial interactions between oil molecules and nanopore surfaces, knowing how much energy is needed to allow oil to be detached from the surface is fundamental to understand the transport and storage behavior of oil in shale,[11] which can determine the favorable recovery techniques and reservoir conditions for oil desorption in terms of thermodynamics. This approach can lead to important implications for oil recovery efforts.

To probe the interfacial interactions at nanoscales, atomistic- and molecular-level characterizations are needed. Both experimental and computational approaches have been

applied to study the hydrocarbon fluid behavior in shale at nanoscale. Extensive experimental studies have been conducted on the shale formation to characterize the organic content[12,13], pore structure[9,14–16], and petrophysics[9,17–19]. These studies aimed to calibrate the empirical models in reservoir engineering to describe the fluid flow[20,21] and to provide implications for reservoir assessment and production optimization.[10] However, it is challenging to interpret the dynamics and kinetics of interface interactions without knowing the molecular scale details given the compositional and structural heterogeneity of shale formations. Understanding the shale systems heavily relies on the characterization technologies to conduct experiments on surfaces and interfaces[22–24] such as Focus Ion Beam Scanning Electron Microscopy (FIB-SEM),[19,25,26] Transmission Electron Microscopy (TEM),[26,27] Atomic Force Microscopy (AFM),[1,20,28] X-ray Diffraction (XRD),[29,30] X-ray microtomography (Micro-CT),[31,32] Nuclear Magnetic Resonance (NMR),[33,34] etc. Implementing these methodologies become challenging at molecular level and even infeasible at atomic scale in order to characterize microscopic phenomena. Unlike experiments, computational simulations can study physical phenomena over a wide range of scale across space and time,[35] directly connecting the microscopic details of a system with macroscopic properties of experimental interest.[36] Due to the intensive computation, Quantum Mechanics (QM) simulations have strict limit on the size, time, and complexity of systems.[35–37] Molecular and atomistic simulations, built on classical molecular mechanics (MM) such as Monte Carlo (MC) and Molecular Dynamics (MD), are more appropriate than QM methods to address the issues of size and complexity of hydrocarbon systems. MC methods are stochastic approach, suitable for analyzing system equilibrium, while MD techniques are deterministic, favorable to study both equilibrium and transport properties of a given system.[36,37] Thus, this study used MD in order to understand the energetics of fluid-rock interactions at nanoscale.

Currently, there are several studies using MD to investigate hydrocarbon fluid interactions with shale minerals and kerogen such as 1) the adsorption, diffusion, and permeation of hydrocarbon fluid in shale kerogen and kerogen analogue;[7,38–44] 2) slippage, displacement, and adsorption of hydrocarbon flow on quartz, calcite slits, and montmorillonite slits;[45–48] 3) detachment of oil cluster from silicate surfaces in surfactant solution.[49] These studies evaluated the effect of nanopores on the properties of hydrocarbon fluid, such as bulk viscosity, contact angle, and slippage. Liu et al 2012 stated that water can penetrate the oil—water interface and form surface water layer on a hydrophilic silica surface, enhancing the oil detachment from the hydrophilic surface. However, the energetic aspect of the hydrocarbon/shale interaction essentially remains intact and hence limited kinetic information is reported.

The present study attempts to test the feasibility of computational approach to evaluate the free energy profile of oil compounds desorption from shale surfaces. Calculation of free energy profile by Umbrella Sampling widely used in computational biology and biochemistry.[50] is adopted in this study to investigate the oil interactions with shale media especially organic kerogen to calculate the free energy changes during the adsorption and desorption processes. We examine the surfaces of kerogen and calcite to evaluate the effect of four different variables including oil polarity (polar vs non-polar oil), oil cluster size (single molecule oil vs 30-molecule oil cluster), surface composition (inorganic calcite mineral vs organic kerogen), and surface water (the presence vs the absence of surface water). Profiling the free energy surface of oil-rock interactions in nanopores provides an insight of hydrocarbon behaviors in unconventional shale reservoir, a multi-phased nano-porous system of rich organic content.

2 Method

2.1 Molecular models for oil, kerogen, and calcite

Crude oil is a mixture of widely varying polar and non-polar compounds as well as their proportions. Typically, crude oil contains over 45% non-polar (e.g. alkanes and cycloalkanes) and less than 15% polar species (e.g. N-, S-, O- and metal-containing compounds).[51,52] Polar components can significantly affect properties of hydrocarbon fluid in reservoir such as viscosity, contact angle, interfacial activity, emulsion, and chemical stability.[2,53,54] The oil-rock interactions are largely attributed by the polar species,[55] particularly in shale since organic phases usually retain more polar components than minerals[2]. Thioalkanes are common sulfur compounds found in crude oils.[56] Shale oil has high content of light oil (C_1-C_9).[57,58] Therefore, we selected 1-octanethiol ($C_8H_{18}S$) with a dipole moment of 2.9 D[59] and its non-polar counterpart n-octane (C_8H_{18}) with no dipole moment as models for polar and nonpolar oil as shown in Figure 2. In addition, to model small oil drop, we prepared two oil clusters consisted of 30 molecules of octanethiol and octane, respectively.

The mineralogy of shale is highly complicated, which contains inorganic and organic constituents. Inorganic phases consist of three major minerals: clays, quartz, and carbonates (calcite and dolomite)[14]. Due to its simple structure, we chose calcite (104) face as a hydrophilic mode of shale inorganic surface. The calcite (104) is a flat stoichiometric surface, which is one of most common mineral faces occurred in both geological and biological systems and has been well studied both computationally and experimentally.[60] The key organic phase in shale involved in the interactions with hydrocarbon is kerogen.[2,61,62] Despite the complexity of kerogen in reservoir formations[63], many studies used graphene to represent kerogen[7,43,44,64–67]. The differences between graphene and kerogen, such as bonding environment of functional groups[68,69] and surface morphology[63], give rise to different chemical and mechanical

properties[69,70]. Changing surface properties can drastically alter the interfacial interactions with hydrocarbons, leading to different simulations results. To capture fundamental properties of kerogen, we employed a molecular fragment $C_{22}H_{13}ON$ derived from type II kerogen to build kerogen surfaces,[38] which is the most common kerogen in hydrocarbon-bearing shale formations[63]. The kerogen molecule has five benzene rings, a secondary amine, and a phenol group, resulting a polar compound. To create kerogen surfaces, 511 kerogen molecules were randomly added into a computational supercell (18,944 atoms in total), quenched from 3000 to 300 K (ramp), and the surfaces were created by insert a vacuum space between the kerogen and then stabilization and relaxation of the surface were followed at 300 K using an NVT ensemble.

The calcite (104) surface in Figure 3(b) was built with 1620 $CaCO_3$ molecule units with a dimension of approximately 7 × 7 × 2 nm with 8,100 atoms. The kerogen surface in Figure 3(a) was built with 511 $C_{22}H_{13}ON$ molecule units with a dimension of approximately 8 × 8 × 3 nm with 18,907 atoms as shown. Because of the ubiquitous presence of water in the reservoir formations, water molecules were added to the fluid. To ensure the complete submergence of their interactions within water, 7,250 and 10,000 water molecules were added to the calcite surface of single oil molecule or oil cluster, respectively; while 7,500 and 10,000 water molecules were placed on kerogen surfaces of single oil molecule or oil cluster, respectively.

A previous experimental study indicates calcite (104) surface exhibits neutral charge due to the stoichiometry of Ca^{2+} and CO_3^{2-}.[71,72] Kerogen surfaces can be negatively charged due to the deprotonation of functional groups, such as OH and NH. However, classical MD models only simulate interatomic interactions by empirical potentials for bond length, angle, and dihedral, whereas formation and breaking of covalent bonds are excluded unless specified by force field. Both calcite and kerogen surfaces maintain electrical neutrality owing to the charge balance of

each model molecule. Layers of alternating Ca^{2+} and CO_3^{2-} on calcite (104) created a well-organized surface of neutral charge, while the benzene rings and polar functional groups of kerogen molecule yielded a highly heterogenous surfaces of kerogen.

2.2 Molecular Dynamics (MD) Simulation and Gibbs Free Energy Profiles

MD simulations in this study were deployed using software package GROningen MAchine for Chemical Simulations (GROMACS).[73] All simulations were under the three-dimensional periodic boundary conditions. The OPLS-AA force field was used to describe oil molecules and kerogen.[74] The SPC potential is used to describe water molecule, which exhibits a dipole moment of 2.27 D, comparable to the experimental measurement 1.85 D.[75] A previously developed force field was used for calcite.[76] All these potentials have been tested and are capable of producing satisfactory results on bulk and interfacial properties, which are consistent with experimental data.[77–79] For a typical umbrella simulation, 1 ns simulation was used for the system to reach equilibrium. Newton's equations of motion were integrated using the leap-frog scheme with a timestep of 1 fs, fast Smooth Particle-Mesh Ewald (SPME) electrostatics, Verlet cutoff-scheme, and temperature coupling using a Nose-Hoover extended ensemble with a coupling constant of 0.1 ps. Simulations were visualized by Visual Molecular Dynamics (VMD) package.[80]

The potential of mean force for the oil interactions with different surfaces was computed by Umbrella Sampling and the Weighted Histogram Analysis Method (WHAM).[81,82] Gromacs package was used to carry out Umbrella Sampling simulations by running separate simulation

windows along the reaction coordinate individually. The simulation windows were generated by simulations pulling the oil into or away from the surfaces regardless of the presence of water.

In each simulation window, umbrella potential, a biased harmonic potential, was applied to the system. For each individual simulation window, we first applied a constraint potential with a force constant 9000 $kJ \cdot mol^{-1} \cdot nm^{-1}$ for 0.1 ns to equilibrate the system, then deployed an umbrella potential with a force constant 9000 $kJ \cdot mol^{-1} \cdot nm^{-2}$ for 0.1 ns up to 0.2 ns if necessary to obtain probability distribution of the given reaction coordinate. With sufficient windows to overlap the entire reaction coordinate space, a free energy profile curve can be calculated by combining data from each window using WHAM.[81,83]

The error analysis on energy profiles was performed by R using LOESS algorithm.[84,85] This method fitted the dataset of each energy profiles and deployed bootstrap technique to calculate confidential interval of 95%. The computed errors listed as shown in Table 1 denoted by brackets. The fluctuations of free energy profile lines as shown in Figure S1 were consistent with the size of the error bar.

3 Results

Free energy surfaces in Figures 4-7 exemplify how the system energy changes as a function of the distance between oil compounds and surfaces. When the oils approach surface, the energy required becomes large due to repulsive interactions. When the oils gradually move away from the surface, the energy reaches the minimal point which is the state of adsorption of the oil at the surfaces. As the distance continuously increases, the energy increase until system

200 reaches the energy plateau region where no additional energies are required to maintain distance
201 between the oils and the surfaces.

202

203 3.1 Interactions of oil molecules with kerogen surface

204 The free energy profiles in Figure 4 and Table 1 show the energy changes as a function of
205 the distance between oil compounds and kerogen surfaces in the presence of water. The
206 desorption energies of these system are 17.0 ± 2.0 kJ/mol and 16.5 ± 3.3 kJ/mol for non-polar
207 and polar single oil molecule and 371± 12.4 kJ/mol and 209 ± 7.0 kJ/mol for non-polar and polar
208 oil clusters, respectively. In the absence of water, it is challenging to maintain oil molecules as a
209 cluster at or above 300 K. To stabilize the oil cluster, a series of identical Umbrella Sampling
210 simulations were carried out under reduced system temperatures to extrapolate the desorption
211 energy to 300 K (detail was discussed in Figure S3). The desorption energies of oil cluster on
212 kerogen surfaces are 437 ± 13.5 kJ/mol for both polar and non-polar (Figure S3). For the single
213 oil molecule, the desorption energies on kerogen in Figure 5 and Table 1 are 23.3 ± 3.5 kJ/mol
214 and 39.5 ± 9.5 kJ/mol for non-polar and polar, respectively.

215

216 3.2 Interactions of oil molecules calcite (104) surface

217 The free energy profiles in Figure 6 shows how free energy changes as a function of the
218 distance between oil compounds and calcite (104) surfaces in water. Unlike the rest free energy
219 profiles (described later), they exhibit a distinct pattern: as the distance increase, the free energy
220 quickly decreased to minimal and maintained at the same level to form a flatland. Such patterns

indicate near zero energies for the desorption of oil molecules on the calcite surface in the presence of water.

For comparison, an identical set of systems without water were simulated, of which the free energy profiles are depicted in Figure 7. The results show that 33.6 ± 3.9 kJ/mol and 18.0 ± 5.5 kJ/mol are required to desorb polar and non-polar oil molecules from calcite surfaces respectively, and 222 ± 36 kJ/mol and 198 ± 42 kJ/mol to desorb polar and non-polar oil clusters, respectively. According to the simulation output trajectory (Fig. S4), the polar molecule was bound to the calcite surface through the thiol functional group –SH, which confirms a previous study on the adsorption of simple organic molecules on calcite (104).[86] In addition, the thiol group –SH of polar oil appears to favor the sites of Ca^{2+} of calcite (104) surface, whereas the non-polar oil shows no preference of absorption sites.

4 Discussion

4.1 Surface effect (kerogen vs calcite)

The simulation results suggest that the desorption energy of oil on calcite surfaces are consistently lower than on kerogen surfaces, suggesting stronger interactions of the oil molecules with kerogen than calcite. The desorption energy is 5.3 to 17 kJ/mol higher for a single oil molecule and 210 to 372 kJ/mol higher for the oil cluster (7.0 to 12.4 kJ/mol per molecule for the oil cluster) at kerogen surface than at the calcite surface regardless of molecular polarity. Both single molecule oil and oil cluster requires higher desorption energy from kerogen than calcite, indicating oil recovery from organic phase of shale requires more energy than the hydrophilic inorganic calcite surface.

Another factor that contributes to the difference between kerogen and calcite surfaces is the surface morphology. Calcite (104) surface is well-structured, which has low surface area. Therefore, calcite has low sorption capacities.[87] The kerogen surface is porous and waxy based on the experimental observations.[63,88] The effective surface area on kerogen would be much higher than calcite, leading to stronger interactions and a higher desorption energy for oil.

4.2 Effect of oil polarity

Molecular polarity plays imperative role in the energetics of oil desorption. For oil adsorbed on the calcite surfaces, polar oil molecules consistently require higher desorption energies than its counterpart non-polar oil owing to the molecular dipole of both polar oil and the hydrophilic nature of calcite surface. The desorption energy for polar oil molecule is about two times of the desorption energy for non-polar oil molecule and the desorption energy for polar oil molecular cluster is about 10% higher than the desorption energy for non-polar oil cluster in the absence of water. However, the effect of polarity is complicated on kerogen surfaces. The desorption energies of the single molecule oil show that the polar oil molecule requires energy about two times of the energy of non-polar per molecule in the absence of water; whereas the desorption energies of polar and nonpolar oil molecules are approximately the same in the presence of water. For 30-molecule oil cluster, our calculation indicates that polar oil cluster requires the same desorption energies as the non-polar oil cluster.

These phenomena can be explained by the dipole interactions. Since there is no free ion in the systems, the intermolecular interactions are controlled by permanent dipole interactions, or Keesom interaction. As shown in Fig S5 a and c, the thiol functional group (–SH, yellow) of

polar oil tend to be in proximity to the functional groups of kerogen molecules such as amine (–NH–, blue) and hydroxyl (–OH, red) upon contact at the interface, which confirms the anticipated dipole interactions. Unlike polar oil, non-polar oil molecules have no dipole moment and therefore a weaker desorption energy than the polar oil molecules. Thus, the affinity of the polar oil molecule with both calcite and kerogen surfaces is stronger than non-polar.[89] This postulation implies that the polar content of shale oil can significantly affect the oil/rock interactions in shale by changing the chemical environment at the interfaces.[53,90–92] This finding suggests that a high polar content in hydrocarbon fluid can bring additional challenges to oil recovery in tight formations of unconventional shale plays.

In the absence of water, similar desorption energies for non-polar and polar oil clusters on kerogen surfaces were similar, which suggests that the molecular polarity has insignificant impact on the interactions between the oil cluster and kerogen surface. As shown in Fig S5, it is possible that the polar oil molecular clusters were formed primarily by the strong dipole interactions between their functional groups thiol –SH, which reduces the exposure of functional groups to the kerogen surfaces and therefore lead to a bonding that is mainly contributed by the interactions of non-polar group of polar molecule with kerogen surface. Another possible explanation is due the heterogenous nature of kerogen surface. The kerogen molecule is a large compound with five non-polar benzene rings and two polar functional groups –OH and –NH–. Therefore, it is possible that the affinity between non-polar groups of kerogen with non-polar oil is similarly strong as the polar groups of kerogen to polar oil.

Moreover, calcite (104) plane cannot be treated as non-polar surface, especially at nanoscale. Previous studies suggested that calcite (104) is overall non-polar because the alternating Ca^{2+} and CO_3^{2-} are closely packed and maintain charge balance.[93,94] Our study shows

that at molecular level the calcite (104) is clearly favors the adsorption of the polar oil than non-polar oil due to the dipole moment possessed in each Ca^{2+} and CO_3^{2-} pair.

4.3 Effect of surface water and oil cluster

The presence of surface water reduces the oil desorption energy on all surface conditions, promoting the oil desorption for all the cases. As discussed previously, calcite is hydrophilic, while kerogen has both hydrophilic and hydrophobic functional groups. The surface water can easily be attracted to the calcite surface and kerogen hydrophilic functional groups. Both water and polar oil molecules have similarly potent dipole moments 2.9 D and 2.27 D, respectively. Water molecules compete with polar oil molecules for adsorption at surfaces with hydrophilic character, and consequently reducing the desorption energy of the oil molecules at the surfaces. The interactions of waters on calcite (104) surfaces were much stronger than on kerogen surfaces, suggesting a weaker hydrophilic nature of kerogen surface than the calcite surface. The affinity between calcite and water is stronger than that between calcite and oil, resulting in a strong oil-repellent surface of calcite in the presence of water.

Our result shows that oil clusters of smaller size require higher desorption energies per molecule than a single molecule of oil. The desorption energies required per molecule for oil clusters are substantially smaller than those of single molecules. For polar oil, the desorption energy of single molecule of oil is 4.6 to 25.2 kJ/mol higher than the desorption energy per molecule in oil cluster, which is 37% to 340% increment of desorption energy per molecule in oil cluster. This difference is mainly attributed to the number of oil molecules that directly interact with the surface. Not all the molecules in the 30-molecule clusters directly interact with

the surfaces, while the single molecule always interacts with the surfaces, which leads to the smaller desorption energies per molecule.

5 Summary and concluding remarks

Molecular Dynamics Simulation is demonstrated to be capable to calculate the energetics of oil/rock interactions at the interfaces. The effects of surface, oil polarity, presence of surface water, numbers of oils in oil molecular cluster on the desorption free energy suggest that 1) the waxy and porous structure of kerogen has a significant contribution to the higher desorption energies owing to the large surface area and strong dipole moments of functional groups than calcite; 2) polar oil compounds require more effort to be recovered than non-polar from both kerogen and calcite surfaces. If the presence of polar content is substantial, it is necessary to treat shale oil as polar mixtures instead of non-polar for effective oil recovery; 3) an single oil molecule or oil molecules larges dispersed in nanopore tends to be more challenging to be recovered than large oil molecular cluster due to stronger interactions with the surfaces than clustered oil molecules; 4) water facilitates the oil desorption by reducing the binding energy between oil and shale rocks, either kerogen or inorganic calcite. Given the desorption process in this study is reversible and is the reserved process of adsorption, the amount of energy required for desorption is the same for adsorption. This study illustrates a computational approach of atomistic scale using realistic models and advanced free energy methods to investigate the energies involved in the oil/rock interactions at fluid-rock interfaces, offering valuable implications for oil recovering from tight reservoirs especially in unconventional shale play.

Conflicts of interest

There are no conflicts to declare.

Acknowledgements

This research used resources of the National Energy Research Scientific Computing Center (NERSC), a U.S. Department of Energy Office of Science User Facility operated under Contract No. DE-AC02-05CH11231. Portions of this research were conducted with high performance computing resources provided by Louisiana State University (http://www.hpc.lsu.edu).

References

(1) Javadpour, F. Nanopores and Apparent Permeability of Gas Flow in Mudrocks (Shales and Siltstone). *J. Can. Pet. Technol.* **2009**, *48* (08), 16–21. https://doi.org/10.2118/09-08-16-DA.

(2) Jarvie, D. M. Shale Resource Systems for Oil and Gas: Part 2—Shale-Oil Resource Systems. **2012**, 89–119. https://doi.org/10.1306/13321447M973489.

(3) Sharma, P.; Ganti, S.; Bhate, N. Effect of Surfaces on the Size-Dependent Elastic State of Nano-Inhomogeneities. *Appl. Phys. Lett.* **2003**, *82* (4), 535–537. https://doi.org/10.1063/1.1539929.

(4) Auffan, M.; Rose, J.; Bottero, J.-Y.; Lowry, G. V.; Jolivet, J.-P.; Wiesner, M. R. Towards a Definition of Inorganic Nanoparticles from an Environmental, Health and Safety Perspective. *Nat. Nanotechnol.* **2009**, *4* (10), 634–641. https://doi.org/10.1038/nnano.2009.242.

(5) Boles, M. A.; Ling, D.; Hyeon, T.; Talapin, D. V. The Surface Science of Nanocrystals. *Nat. Mater.* **2016**, *15* (2), 141–153. https://doi.org/10.1038/nmat4526.

(6) Wang, Y. Nanogeochemistry: Nanostructures, Emergent Properties and Their Control on Geochemical Reactions and Mass Transfers. *Chem. Geol.* **2014**, *378–379*, 1–23. https://doi.org/10.1016/j.chemgeo.2014.04.007.

(7) Falk, K.; Coasne, B.; Pellenq, R.; Ulm, F.-J.; Bocquet, L. Subcontinuum Mass Transport of Condensed Hydrocarbons in Nanoporous Media. *Nat. Commun.* **2015**, *6*, 6949. https://doi.org/10.1038/ncomms7949.

(8) Javadpour, F.; Fisher, D.; Unsworth, M. Nanoscale Gas Flow in Shale Gas Sediments. *J. Can. Pet. Technol.* **2007**, *46* (10). https://doi.org/10.2118/07-10-06.

(9) Sondergeld, C. H.; Ambrose, R. J.; Rai, C. S.; Moncrieff, J. Micro-Structural Studies of Gas Shales; Society of Petroleum Engineers, 2010. https://doi.org/10.2118/131771-MS.

(10) Wang, F. P.; Reed, R. M. Pore Networks and Fluid Flow in Gas Shales; Society of Petroleum Engineers, 2009. https://doi.org/10.2118/124253-MS.

(11) Pohorille, A.; Chipot, C. Summary and Outlook. In *Free Energy Calculations: Theory and Applications in Chemistry and Biology*; Chipot, C., Pohorille, A., Eds.; Springer Series in CHEMICAL PHYSICS; Springer Berlin Heidelberg: Berlin, Heidelberg, 2007; pp 503–513. https://doi.org/10.1007/978-3-540-38448-9_14.

(12) Zhang, T.; Ellis, G. S.; Ruppel, S. C.; Milliken, K.; Yang, R. Effect of Organic-Matter Type and Thermal Maturity on Methane Adsorption in Shale-Gas Systems. *Org. Geochem.* **2012**, *47*, 120–131. https://doi.org/10.1016/j.orggeochem.2012.03.012.

(13) Hutton, A. C.; Kantsler, A. J.; Cook, A. C.; McKirdy, D. M. ORGANIC MATTER IN OIL SHALES. *APPEA J.* **1980**, *20* (1), 44–67. https://doi.org/10.1071/aj79005.

(14) Ross, D. J. K.; Marc Bustin, R. The Importance of Shale Composition and Pore Structure upon Gas Storage Potential of Shale Gas Reservoirs. *Mar. Pet. Geol.* **2009**, *26* (6), 916–927. https://doi.org/10.1016/j.marpetgeo.2008.06.004.

(15) Loucks, R. G.; Reed, R. M.; Ruppel, S. C.; Hammes, U. Spectrum of Pore Types and Networks in Mudrocks and a Descriptive Classification for Matrix-Related Mudrock PoresSpectrum of Pore Types and Networks In Mudrocks. *AAPG Bull.* **2012**, *96* (6), 1071–1098. https://doi.org/10.1306/08171111061.

(16) Clarkson, C. R.; Solano, N.; Bustin, R. M.; Bustin, A. M. M.; Chalmers, G. R. L.; He, L.; Melnichenko, Y. B.; Radliński, A. P.; Blach, T. P. Pore Structure Characterization of North American Shale Gas Reservoirs Using USANS/SANS, Gas Adsorption, and Mercury Intrusion. *Fuel* **2013**, *103*, 606–616. https://doi.org/10.1016/j.fuel.2012.06.119.

(17) Passey, Q. R.; Bohacs, K.; Esch, W. L.; Klimentidis, R.; Sinha, S. From Oil-Prone Source Rock to Gas-Producing Shale Reservoir - Geologic and Petrophysical Characterization of Unconventional Shale Gas Reservoirs; Society of Petroleum Engineers, 2010. https://doi.org/10.2118/131350-MS.

(18) Vernik, L.; Milovac, J. Rock Physics of Organic Shales. *Lead. Edge* **2011**, *30* (3), 318–323. https://doi.org/10.1190/1.3567263.

(19) Milliken, K. L.; Rudnicki, M.; Awwiller, D. N.; Zhang, T. Organic Matter–Hosted Pore System, Marcellus Formation (Devonian), PennsylvaniaGeohorizon. *AAPG Bull.* **2013**, *97* (2), 177–200. https://doi.org/10.1306/07231212048.

(20) Shabro, V.; Torres-Verdin, C.; Javadpour, F. Numerical Simulation of Shale-Gas Production: From Pore-Scale Modeling of Slip-Flow, Knudsen Diffusion, and Langmuir Desorption to Reservoir Modeling of Compressible Fluid; Society of Petroleum Engineers, 2011. https://doi.org/10.2118/144355-MS.

(21) Wu, K.; Li, X.; Wang, C.; Yu, W.; Chen, Z. Model for Surface Diffusion of Adsorbed Gas in Nanopores of Shale Gas Reservoirs. *Ind. Eng. Chem. Res.* **2015**, *54* (12), 3225–3236. https://doi.org/10.1021/ie504030v.

(22) Zaera, F. Probing Liquid/Solid Interfaces at the Molecular Level. *Chem. Rev.* **2012**, *112* (5), 2920–2986. https://doi.org/10.1021/cr2002068.

(23) *Surface Analysis Methods in Materials Science*; O'Connor, J., Sexton, B., Smart, R., Eds.; Springer Series in Surface Sciences; Springer-Verlag: Berlin Heidelberg, 1992.

(24) Mineralogical Society of America - Mineral-Water Interface Geochemistry http://www.minsocam.org/msa/rim/rim23.html (accessed Mar 13, 2019).

(25) Milner, M.; McLin, R.; Petriello, J. Imaging Texture and Porosity in Mudstones and Shales: Comparison of Secondary and Ion-Milled Backscatter SEM Methods; Society of Petroleum Engineers, 2010. https://doi.org/10.2118/138975-MS.

(26) Curtis, M. E.; Ambrose, R. J.; Sondergeld, C. H.; Rai, C. S. Transmission and Scanning Electron Microscopy Investigation of Pore Connectivity of Gas Shales on the Nanoscale; Society of Petroleum Engineers, 2011. https://doi.org/10.2118/144391-MS.

(27) Bernard, S.; Horsfield, B.; Schulz, H.-M.; Wirth, R.; Schreiber, A.; Sherwood, N. Geochemical Evolution of Organic-Rich Shales with Increasing Maturity: A STXM and TEM Study of the Posidonia Shale (Lower Toarcian, Northern Germany). *Mar. Pet. Geol.* **2012**, *31* (1), 70–89. https://doi.org/10.1016/j.marpetgeo.2011.05.010.

(28) Javadpour, F.; Moravvej Farshi, M.; Amrein, M. Atomic-Force Microscopy: A New Tool for Gas-Shale Characterization. *J. Can. Pet. Technol.* **2012**, *51* (04), 236–243. https://doi.org/10.2118/161015-PA.

(29) Bhargava, S.; Awaja, F.; Subasinghe, N. D. Characterisation of Some Australian Oil Shale Using Thermal, X-Ray and IR Techniques. *Fuel* **2005**, *84* (6), 707–715. https://doi.org/10.1016/j.fuel.2004.11.013.

(30) Elgmati, M. M.; Zhang, H.; Bai, B.; Flori, R. E.; Qu, Q. Submicron-Pore Characterization of Shale Gas Plays; Society of Petroleum Engineers, 2011. https://doi.org/10.2118/144050-MS.

(31) Tiwari, P.; Deo, M.; Lin, C. L.; Miller, J. D. Characterization of Oil Shale Pore Structure before and after Pyrolysis by Using X-Ray Micro CT. *Fuel* **2013**, *107*, 547–554. https://doi.org/10.1016/j.fuel.2013.01.006.

(32) Duliu, O. G. Computer Axial Tomography in Geosciences: An Overview. *Earth-Sci. Rev.* **1999**, *48* (4), 265–281. https://doi.org/10.1016/S0012-8252(99)00056-2.

(33) Kadayam Viswanathan, R. K.; Cao Minh, C.; Zielinski, L.; Vissapragada, B.; Akkurt, R.; Song, Y.-Q.; Liu, C.; Jones, S.; Blair, E. Characterization of Gas Dynamics in Kerogen Nanopores by NMR; Society of Petroleum Engineers, 2011. https://doi.org/10.2118/147198-MS.

(34) Korb, J.-P.; Nicot, B.; Louis-Joseph, A.; Bubici, S.; Ferrante, G. Dynamics and Wettability of Oil and Water in Oil Shales. *J. Phys. Chem. C* **2014**, *118* (40), 23212–23218. https://doi.org/10.1021/jp508659e.

(35) Cygan, R. T. Molecular Modeling in Mineralogy and Geochemistry. *Rev. Mineral. Geochem.* **2001**, *42* (1), 1–35. https://doi.org/10.2138/rmg.2001.42.1.

(36) Allen, M.; Tildesley, D. *Computer Simulation of Liquids*, Second Edition.; Oxford University Press: Oxford, New York, 2017.

(37) Frenkel, D.; Smit, B. *Understanding Molecular Simulation: From Algorithms to Applications*, Second Edition.; Academic Press: San Diego, 2002.

(38) Collell, J.; Galliero, G.; Gouth, F.; Montel, F.; Pujol, M.; Ungerer, P.; Yiannourakou, M. Molecular Simulation and Modelisation of Methane/Ethane Mixtures Adsorption onto a Microporous Molecular Model of Kerogen under Typical Reservoir Conditions. *Microporous Mesoporous Mater.* **2014**, *197*, 194–203. https://doi.org/10.1016/j.micromeso.2014.06.016.

(39) Collell, J.; Galliero, G.; Vermorel, R.; Ungerer, P.; Yiannourakou, M.; Montel, F.; Pujol, M. Transport of Multicomponent Hydrocarbon Mixtures in Shale Organic Matter by Molecular Simulations. *J. Phys. Chem. C* **2015**, *119* (39), 22587–22595. https://doi.org/10.1021/acs.jpcc.5b07242.

(40) Collell, J.; Ungerer, P.; Galliero, G.; Yiannourakou, M.; Montel, F.; Pujol, M. Molecular Simulation of Bulk Organic Matter in Type II Shales in the Middle of the Oil Formation Window. *Energy Fuels* **2014**, *28* (12), 7457–7466. https://doi.org/10.1021/ef5021632.

(41) Sui, H.; Yao, J. Effect of Surface Chemistry for CH4/CO2 Adsorption in Kerogen: A Molecular Simulation Study. *J. Nat. Gas Sci. Eng.* **2016**, *31*, 738–746. https://doi.org/10.1016/j.jngse.2016.03.097.

(42) Yiannourakou, M.; Ungerer, P.; Leblanc, B.; Rozanska, X.; Saxe, P.; Vidal-Gilbert, S.; Gouth, F.; Montel, F. Molecular Simulation of Adsorption in Microporous Materials. *Oil Gas Sci. Technol. – Rev. D'IFP Energ. Nouv.* **2013**, *68* (6), 977–994. https://doi.org/10.2516/ogst/2013134.

(43) Lee, T.; Bocquet, L.; Coasne, B. Activated Desorption at Heterogeneous Interfaces and Long-Time Kinetics of Hydrocarbon Recovery from Nanoporous Media. *Nat. Commun.* **2016**, *7*, 11890. https://doi.org/10.1038/ncomms11890.

(44) Ambrose, R. J.; Hartman, R. C.; Diaz-Campos, M.; Akkutlu, I. Y.; Sondergeld, C. H. Shale Gas-in-Place Calculations Part I: New Pore-Scale Considerations. *SPE J.* **2012**, *17* (01), 219–229. https://doi.org/10.2118/131772-PA.

(45) Wang, S.; Javadpour, F.; Feng, Q. Molecular Dynamics Simulations of Oil Transport through Inorganic Nanopores in Shale. *Fuel* **2016**, *171*, 74–86. https://doi.org/10.1016/j.fuel.2015.12.071.

(46) Wang, S.; Feng, Q.; Javadpour, F.; Yang, Y.-B. Breakdown of Fast Mass Transport of Methane through Calcite Nanopores. *J. Phys. Chem. C* **2016**, *120* (26), 14260–14269. https://doi.org/10.1021/acs.jpcc.6b05511.

(47) Zheng, H.; Du, Y.; Xue, Q.; Zhu, L.; Li, X.; Lu, S.; Jin, Y. Surface Effect on Oil Transportation in Nanochannel: A Molecular Dynamics Study. *Nanoscale Res. Lett.* **2017**, *12* (1), 413. https://doi.org/10.1186/s11671-017-2161-2.

(48) Underwood, T.; Erastova, V.; Cubillas, P.; Greenwell, H. C. Molecular Dynamic Simulations of Montmorillonite–Organic Interactions under Varying Salinity: An Insight into Enhanced Oil Recovery. *J. Phys. Chem. C* **2015**, *119* (13), 7282–7294. https://doi.org/10.1021/acs.jpcc.5b00555.

(49) Liu, Q.; Yuan, S.; Yan, H.; Zhao, X. Mechanism of Oil Detachment from a Silica Surface in Aqueous Surfactant Solutions: Molecular Dynamics Simulations. *J. Phys. Chem. B* **2012**, *116* (9), 2867–2875. https://doi.org/10.1021/jp2118482.

(50) Kästner, J. Umbrella Sampling. *Wiley Interdiscip. Rev. Comput. Mol. Sci.* **2011**, *1* (6), 932–942. https://doi.org/10.1002/wcms.66.

(51) Hughey, C. A.; Rodgers, R. P.; Marshall, A. G.; Qian, K.; Robbins, W. K. Identification of Acidic NSO Compounds in Crude Oils of Different Geochemical Origins by Negative Ion Electrospray Fourier Transform Ion Cyclotron Resonance Mass Spectrometry. *Org. Geochem.* **2002**, *33* (7), 743–759. https://doi.org/10.1016/S0146-6380(02)00038-4.
(52) Hyne, N. J. *Nontechnical Guide to Petroleum Geology, Exploration, Drilling, and Production*; PennWell Corporation: Tulsa, Okla., 2012.
(53) Buckley, J. S.; Liu, Y.; Monsterleet, S. Mechanisms of Wetting Alteration by Crude Oils. *SPE J.* **1998**, *3* (01), 54–61. https://doi.org/10.2118/37230-PA.
(54) Sayyouh, M. H.; Hemeida, A. M.; Al-Blehed, M. S.; Desouky, S. M. Role of Polar Compounds in Crude Oils on Rock Wettability. *J. Pet. Sci. Eng.* **1991**, *6* (3), 225–233. https://doi.org/10.1016/0920-4105(91)90015-F.
(55) Speight, J. G. The Chemical and Physical Structure of Petroleum: Effects on Recovery Operations. *J. Pet. Sci. Eng.* **1999**, *22* (1), 3–15. https://doi.org/10.1016/S0920-4105(98)00051-5.
(56) Composition, Classification, and Properties of Petroleum. In *Chemistry of Fossil Fuels and Biofuels*; Schobert, H., Ed.; Cambridge Series in Chemical Engineering; Cambridge University Press: Cambridge, 2013; pp 174–191. https://doi.org/10.1017/CBO9780511844188.012.
(57) Mango, F. D. The Light Hydrocarbons in Petroleum: A Critical Review. *Org. Geochem.* **1997**, *26* (7), 417–440. https://doi.org/10.1016/S0146-6380(97)00031-4.
(58) Yanik, J.; Yüksel, M.; Sağlam, M.; Olukçu, N.; Bartle, K.; Frere, B. Characterization of the Oil Fractions of Shale Oil Obtained by Pyrolysis and Supercritical Water Extraction. *Fuel* **1995**, *74* (1), 46–50. https://doi.org/10.1016/0016-2361(94)P4329-Z.
(59) Kvashnin, D. G.; Antipina, L. Y.; Sorokin, P. B.; Tenne, R.; Golberg, D. Theoretical Aspects of WS2 Nanotube Chemical Unzipping. *Nanoscale* **2014**, *6* (14), 8400–8404. https://doi.org/10.1039/C4NR00437J.
(60) Kerisit, S.; Parker, S. C. Free Energy of Adsorption of Water and Metal Ions on the {10$\bar{1}$4} Calcite Surface. *J. Am. Chem. Soc.* **2004**, *126* (32), 10152–10161. https://doi.org/10.1021/ja0487776.
(61) Curtis, J. B. Fractured Shale-Gas Systems. *AAPG Bull.* **2002**, *86* (11), 1921–1938. https://doi.org/10.1306/61EEDDBE-173E-11D7-8645000102C1865D.
(62) Jarvie, D. M.; Hill, R. J.; Ruble, T. E.; Pollastro, R. M. Unconventional Shale-Gas Systems: The Mississippian Barnett Shale of North-Central Texas as One Model for Thermogenic Shale-Gas Assessment. *AAPG Bull.* **2007**, *91* (4), 475–499. https://doi.org/10.1306/12190606068.
(63) Vandenbroucke, M.; Largeau, C. Kerogen Origin, Evolution and Structure. *Org. Geochem.* **2007**, *38* (5), 719–833. https://doi.org/10.1016/j.orggeochem.2007.01.001.
(64) Hu, Y.; Devegowda, D.; Striolo, A.; Phan, A.; Ho, T. A.; Civan, F.; Sigal, R. F. Microscopic Dynamics of Water and Hydrocarbon in Shale-Kerogen Pores of Potentially Mixed Wettability. *SPE J.* **2014**, *20* (01), 112–124. https://doi.org/10.2118/167234-PA.
(65) Firouzi, M.; Rupp, E. C.; Liu, C. W.; Wilcox, J. Molecular Simulation and Experimental Characterization of the Nanoporous Structures of Coal and Gas Shale. *Int. J. Coal Geol.* **2014**, *121*, 123–128. https://doi.org/10.1016/j.coal.2013.11.003.
(66) Falk, K.; Pellenq, R.; Ulm, F. J.; Coasne, B. Effect of Chain Length and Pore Accessibility on Alkane Adsorption in Kerogen. *Energy Fuels* **2015**, *29* (12), 7889–7896. https://doi.org/10.1021/acs.energyfuels.5b02015.
(67) Ambrose, R. J.; Hartman, R. C.; Diaz Campos, M.; Akkutlu, I. Y.; Sondergeld, C. New Pore-Scale Considerations for Shale Gas in Place Calculations; Society of Petroleum Engineers, 2010. https://doi.org/10.2118/131772-MS.
(68) Orendt, A. M.; Pimienta, I. S. O.; Badu, S. R.; Solum, M. S.; Pugmire, R. J.; Facelli, J. C.; Locke, D. R.; Chapman, K. W.; Chupas, P. J.; Winans, R. E. Three-Dimensional Structure of the Siskin Green River

Oil Shale Kerogen Model: A Comparison between Calculated and Observed Properties. *Energy Fuels* **2013**, *27* (2), 702–710. https://doi.org/10.1021/ef3017046.

(69) Bousige, C.; Ghimbeu, C. M.; Vix-Guterl, C.; Pomerantz, A. E.; Suleimenova, A.; Vaughan, G.; Garbarino, G.; Feygenson, M.; Wildgruber, C.; Ulm, F.-J.; et al. Realistic Molecular Model of Kerogen's Nanostructure. *Nat. Mater.* **2016**, *15* (5), 576–582. https://doi.org/10.1038/nmat4541.

(70) Pei, Q.-X.; Zhang, Y.-W.; Shenoy, V. B. Mechanical Properties of Methyl Functionalized Graphene: A Molecular Dynamics Study. *Nanotechnology* **2010**, *21* (11), 115709. https://doi.org/10.1088/0957-4484/21/11/115709.

(71) Lee, S. S.; Heberling, F.; Sturchio, N. C.; Eng, P. J.; Fenter, P. Surface Charge of the Calcite (104) Terrace Measured by Rb+ Adsorption in Aqueous Solutions Using Resonant Anomalous X-Ray Reflectivity. *J. Phys. Chem. C* **2016**, *120* (28), 15216–15223. https://doi.org/10.1021/acs.jpcc.6b04364.

(72) Wolthers, M.; Tommaso, D. D.; Du, Z.; Leeuw, N. H. de. Calcite Surface Structure and Reactivity: Molecular Dynamics Simulations and Macroscopic Surface Modelling of the Calcite –Water Interface. *Phys. Chem. Chem. Phys.* **2012**, *14* (43), 15145–15157. https://doi.org/10.1039/C2CP42290E.

(73) Berendsen, H. J. C.; van der Spoel, D.; van Drunen, R. GROMACS: A Message-Passing Parallel Molecular Dynamics Implementation. *Comput. Phys. Commun.* **1995**, *91* (1), 43–56. https://doi.org/10.1016/0010-4655(95)00042-E.

(74) Robertson, M. J.; Tirado-Rives, J.; Jorgensen, W. L. Improved Peptide and Protein Torsional Energetics with the OPLS-AA Force Field. *J. Chem. Theory Comput.* **2015**, *11* (7), 3499–3509. https://doi.org/10.1021/acs.jctc.5b00356.

(75) Berendsen, H. J. C.; Postma, J. P. M.; van Gunsteren, W. F.; Hermans, J. Interaction Models for Water in Relation to Protein Hydration. In *Intermolecular Forces: Proceedings of the Fourteenth Jerusalem Symposium on Quantum Chemistry and Biochemistry Held in Jerusalem, Israel, April 13–16, 1981*; Pullman, B., Ed.; The Jerusalem Symposia on Quantum Chemistry and Biochemistry; Springer Netherlands: Dordrecht, 1981; pp 331–342. https://doi.org/10.1007/978-94-015-7658-1_21.

(76) Raiteri, P.; Gale, J. D.; Quigley, D.; Rodger, P. M. Derivation of an Accurate Force-Field for Simulating the Growth of Calcium Carbonate from Aqueous Solution: A New Model for the Calcite−Water Interface. *J. Phys. Chem. C* **2010**, *114* (13), 5997–6010. https://doi.org/10.1021/jp910977a.

(77) Geissbühler, P.; Fenter, P.; DiMasi, E.; Srajer, G.; Sorensen, L. B.; Sturchio, N. C. Three-Dimensional Structure of the Calcite–Water Interface by Surface X-Ray Scattering. *Surf. Sci.* **2004**, *573* (2), 191–203. https://doi.org/10.1016/j.susc.2004.09.036.

(78) Wolf, G.; Lerchner, J.; Schmidt, H.; Gamsjäger, H.; Königsberger, E.; Schmidt, P. Thermodynamics of CaCO3 Phase Transitions. *J. Therm. Anal. Calorim.* **1996**, *46* (2), 353–359. https://doi.org/10.1007/BF02135013.

(79) Wolf, G.; Königsberger, E.; Schmidt, H. G.; Königsberger, L.-C.; Gamsjäger, H. Thermodynamic Aspects of the Vaterite-Calcite Phase Transition. *J. Therm. Anal. Calorim.* **2000**, *60* (2), 463–472. https://doi.org/10.1023/A:1010114131577.

(80) Humphrey, W.; Dalke, A.; Schulten, K. VMD: Visual Molecular Dynamics. *J. Mol. Graph.* **1996**, *14* (1), 33–38. https://doi.org/10.1016/0263-7855(96)00018-5.

(81) Kumar, S.; Rosenberg, J. M.; Bouzida, D.; Swendsen, R. H.; Kollman, P. A. THE Weighted Histogram Analysis Method for Free-Energy Calculations on Biomolecules. I. The Method. *J. Comput. Chem.* **1992**, *13* (8), 1011–1021. https://doi.org/10.1002/jcc.540130812.

(82) Roux, B. The Calculation of the Potential of Mean Force Using Computer Simulations. *Comput. Phys. Commun.* **1995**, *91* (1), 275–282. https://doi.org/10.1016/0010-4655(95)00053-I.

(83) Hub, J. S.; de Groot, B. L.; van der Spoel, D. G_wham—A Free Weighted Histogram Analysis Implementation Including Robust Error and Autocorrelation Estimates. *J. Chem. Theory Comput.* **2010**, *6* (12), 3713–3720. https://doi.org/10.1021/ct100494z.
(84) Cleveland, W. S. Robust Locally Weighted Regression and Smoothing Scatterplots. *J. Am. Stat. Assoc.* **1979**, *74* (368), 829–836. https://doi.org/10.1080/01621459.1979.10481038.
(85) R Core Team. *R: A Language and Environment for Statistical Computing*; R Foundation for Statistical Computing: Vienna, Austria, 2019.
(86) Hakim, S. S.; Olsson, M. H. M.; Sørensen, H. O.; Bovet, N.; Bohr, J.; Feidenhans'l, R.; Stipp, S. L. S. Interactions of the Calcite {10.4} Surface with Organic Compounds: Structure and Behaviour at Mineral – Organic Interfaces. *Sci. Rep.* **2017**, *7* (1), 7592. https://doi.org/10.1038/s41598-017-06977-4.
(87) Ross, D. J. K.; Bustin, R. M. Shale Gas Potential of the Lower Jurassic Gordondale Member, Northeastern British Columbia, Canada. *Bull. Can. Pet. Geol.* **2007**, *55* (1), 51–75. https://doi.org/10.2113/gscpgbull.55.1.51.
(88) Loucks, R. G.; Reed, R. M.; Ruppel, S. C.; Jarvie, D. M. Morphology, Genesis, and Distribution of Nanometer-Scale Pores in Siliceous Mudstones of the Mississippian Barnett Shale. *J. Sediment. Res.* **2009**, *79* (12), 848–861. https://doi.org/10.2110/jsr.2009.092.
(89) Madsen, L.; Grahl-Madsen, L.; Grøn, C.; Lind, I.; Engell, J. Adsorption of Polar Aromatic Hydrocarbons on Synthetic Calcite. *Org. Geochem.* **1996**, *24* (12), 1151–1155. https://doi.org/10.1016/S0146-6380(96)00096-4.
(90) Crocker, M. E.; Marchin, L. M. Wettability and Adsorption Characteristics of Crude-Oil Asphaltene and Polar Fractions. *J. Pet. Technol.* **1988**, *40* (04), 470–474. https://doi.org/10.2118/14885-PA.
(91) He, L.; Lin, F.; Li, X.; Sui, H.; Xu, Z. Interfacial Sciences in Unconventional Petroleum Production: From Fundamentals to Applications. *Chem. Soc. Rev.* **2015**, *44* (15), 5446–5494. https://doi.org/10.1039/C5CS00102A.
(92) Morrow, N. R. Wettability and Its Effect on Oil Recovery. *J. Pet. Technol.* **1990**, *42* (12), 1,476-1,484. https://doi.org/10.2118/21621-PA.
(93) García Carmona, J.; Gómez Morales, J.; Rodríguez Clemente, R. Rhombohedral–Scalenohedral Calcite Transition Produced by Adjusting the Solution Electrical Conductivity in the System Ca(OH)2–CO2–H2O. *J. Colloid Interface Sci.* **2003**, *261* (2), 434–440. https://doi.org/10.1016/S0021-9797(03)00149-8.
(94) Shen, J.-W.; Li, C.; van der Vegt, N. F. A.; Peter, C. Understanding the Control of Mineralization by Polyelectrolyte Additives: Simulation of Preferential Binding to Calcite Surfaces. *J. Phys. Chem. C* **2013**, *117* (13), 6904–6913. https://doi.org/10.1021/jp402341w.

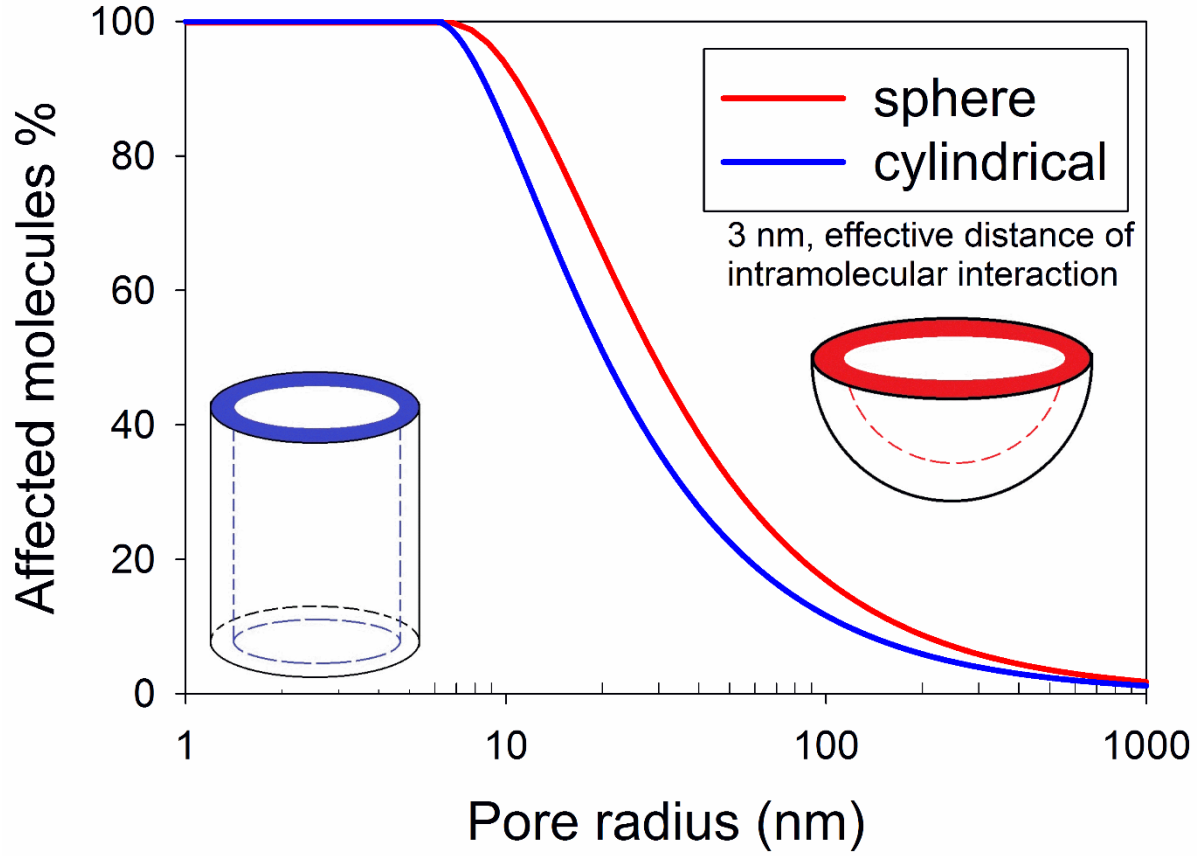

609

610 Figure 1. Effect of intermolecular interaction on the fluid confined in nanostructures.

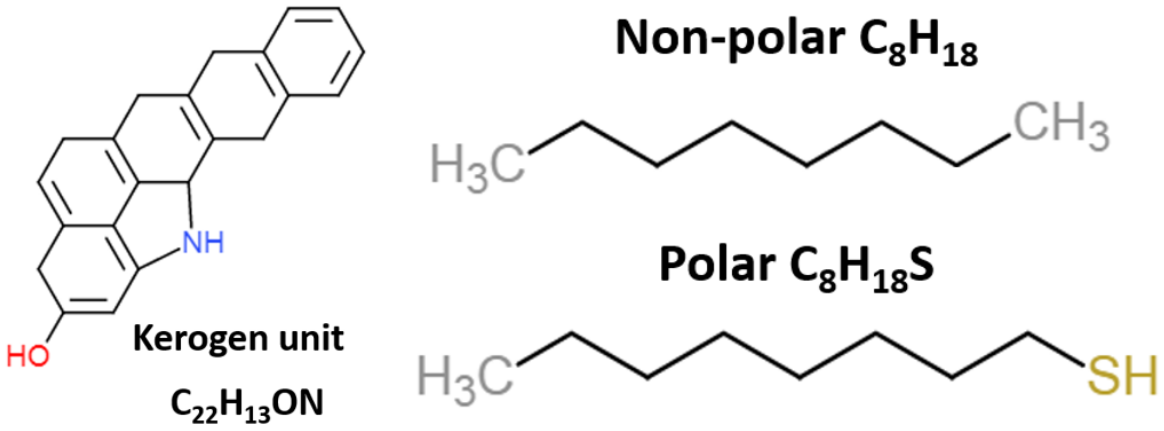

Figure 2. Molecular structure of type II kerogen fragment (left), non-polar oil n-octane (right top), and polar oil 1-octanethiol (right bottom).

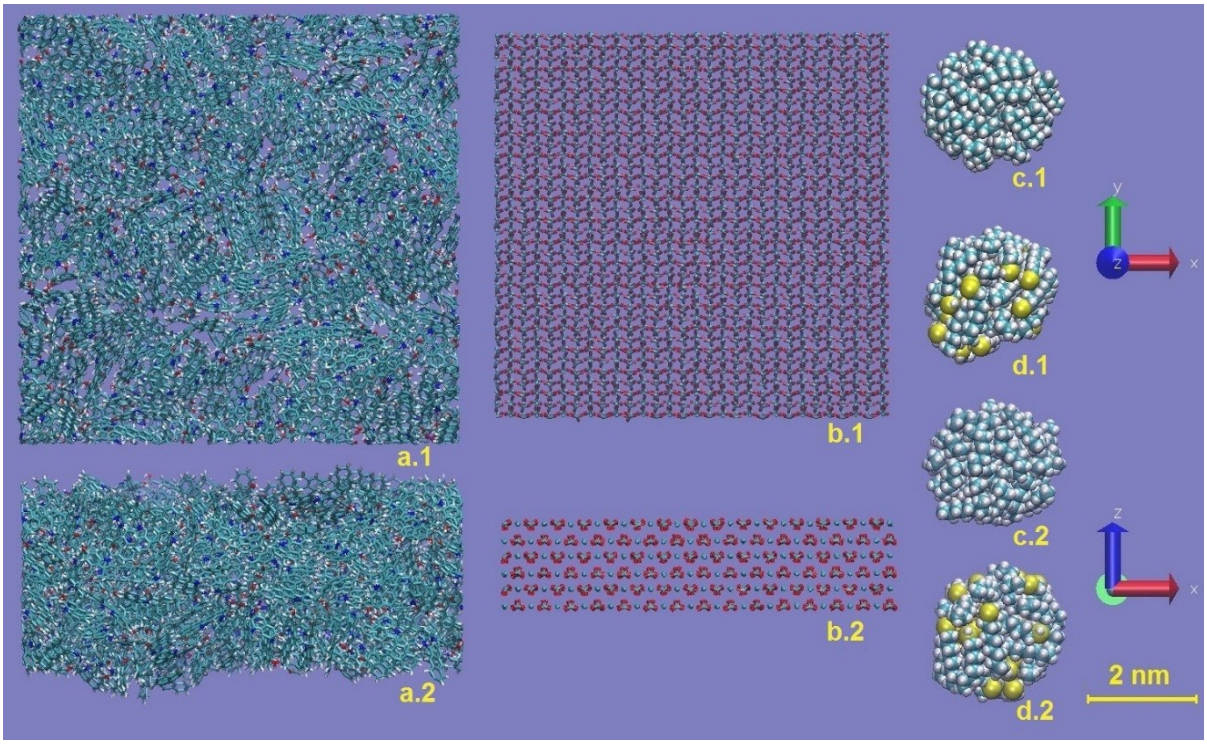

Figure 3. Kerogen slab (a), calcite (104) slab (b), 30-molecule non-polar oil cluster (c), and 30-molecule polar oil cluster (d). "x.1" and "x.2" denote different orientations.

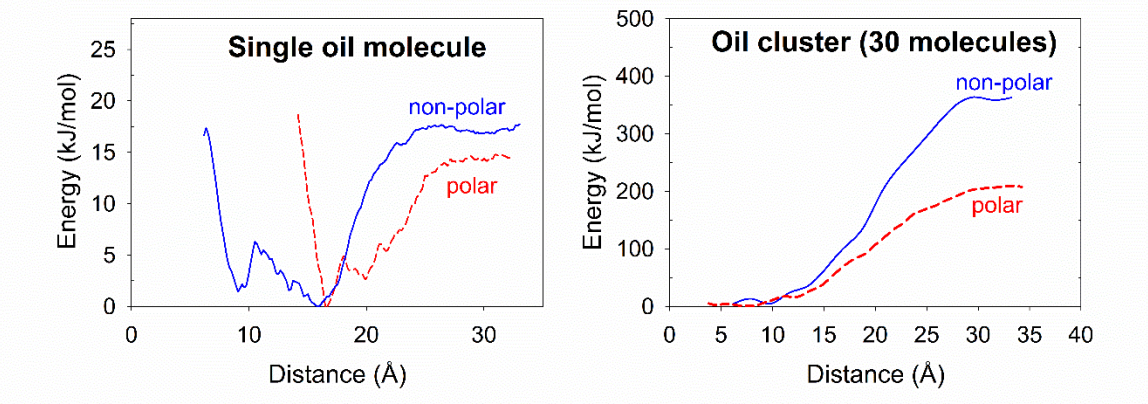

Figure 4. Free energy surfaces of single molecule of polar or non-polar oil on kerogen surface with water (left); Free energy surfaces of oil drop of 30 polar or non-polar oil molecules on kerogen surface with water (right).

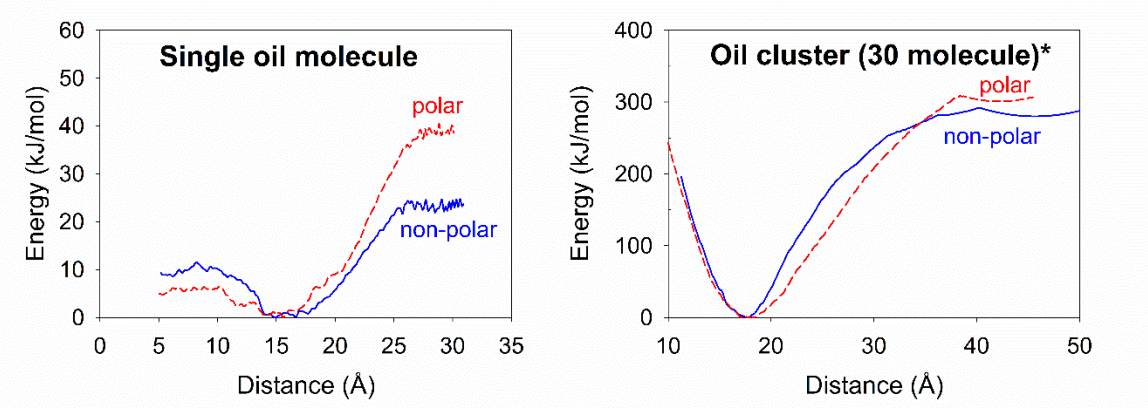

Figure 5. Free energy surfaces of single molecule of polar and non-polar oil on kerogen surface without water (left); free energy surfaces of oil drop of 30 polar or non-polar oil molecules on kerogen surface without water (right). *indicates the simulations were prepared at 200K due to the technical issues as described in the discussion.

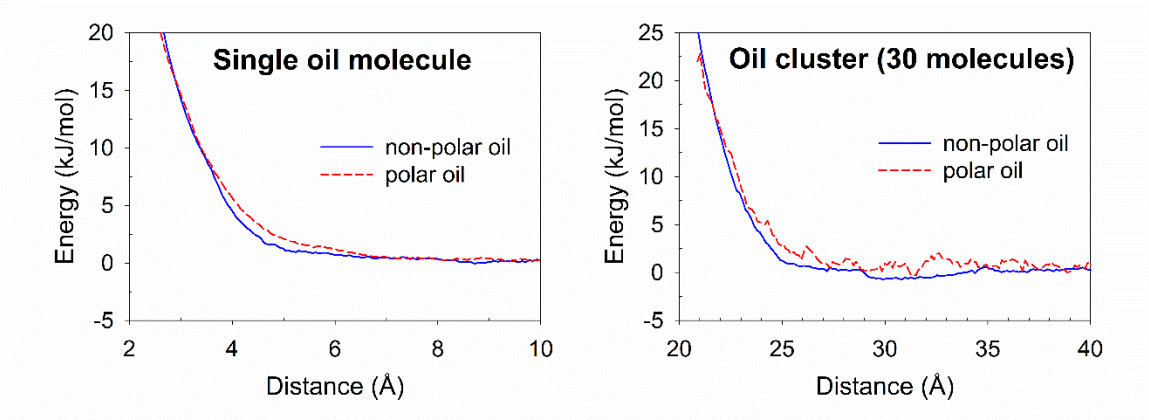

630

631 Figure 6. Free energy surfaces of single molecule and 30-molecule cluster of polar or non-polar oil on
632 calcite surface in the presence of water.

633

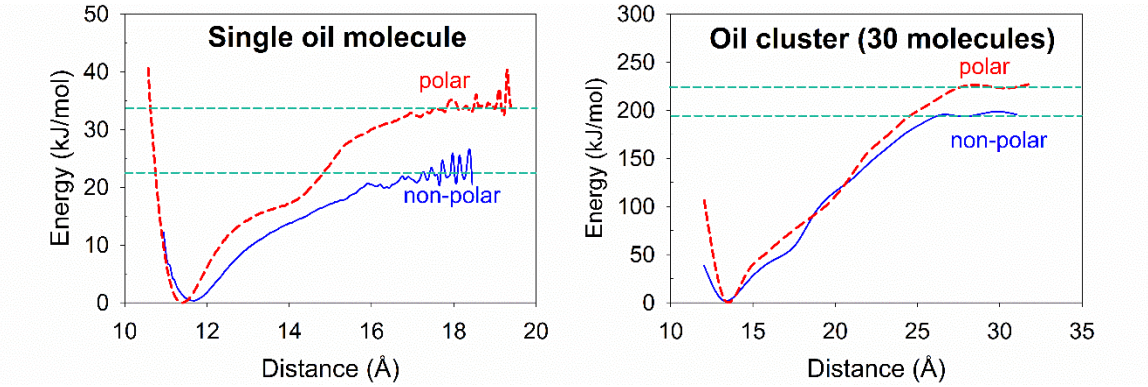

Figure 7. Free energy surfaces of single molecule of polar or non-polar oil on calcite surface without water (left); free energy surfaces of oil drop of polar or non-polar oil on calcite surface without water (right).

Table 1. Desorption energy of single molecule oil droplet and 30-molecule oil drop on calcite and kerogen surface under 300 K. The ( ) denotes the errors propagated from the output data of WHAM.

Desorption energy (kJ/mol)		Kerogen with water	Kerogen	Calcite with water	Calcite
Non-polar	Single molecule	17.0 (2.0)	23.3 (3.5)	0	18.0 (5.5)
	Cluster	372 (13.8)	438 (13. 5)	0	198 (42)
Polar oil	Single molecule	16.5 (3.3)	39.5 (9.5)	0	33.6 (3.9)
	Cluster	210 (11.4)	438 (13.5)	0	222 (36)
Desorption energy per molecule (kJ/mol)		Kerogen with water	Kerogen	Calcite with water	Calcite
Non-polar	Single molecule	17.0 (2.0)	23.3 (3.5)	0	18.0 (5.5)
	Cluster	12.4 (0.46)	14.6 (0.45)	0	6.6 (1.4)
Polar oil	Single molecule	16.5 (3.3)	39.5 (9.5)	0	33.6 (3.9)
	Cluster	7.0 (0.38)	14.6 (0.45)	0	7.4 (1.2)

Supplement Information

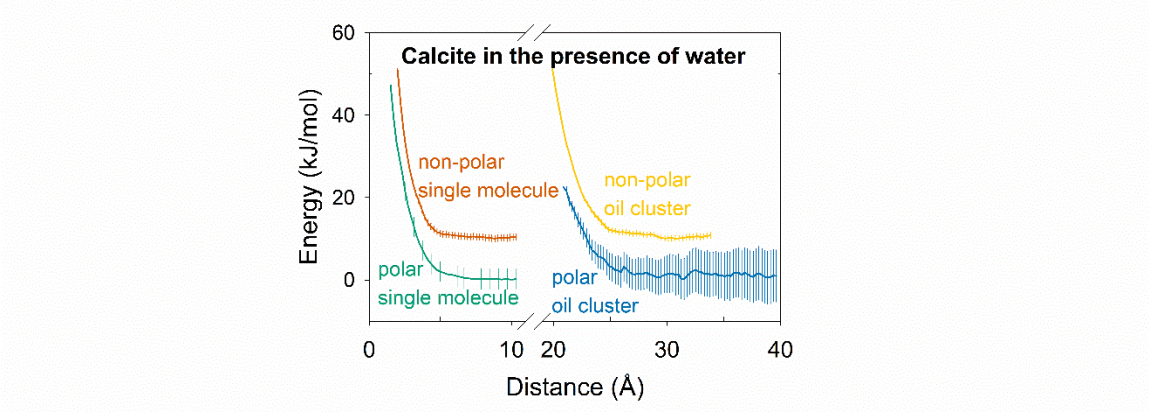

Fig S1. Free energy surfaces of oil drop of polar or non-polar oil on calcite surface with water. The density of displayed data is reduced for visual clarity.

646

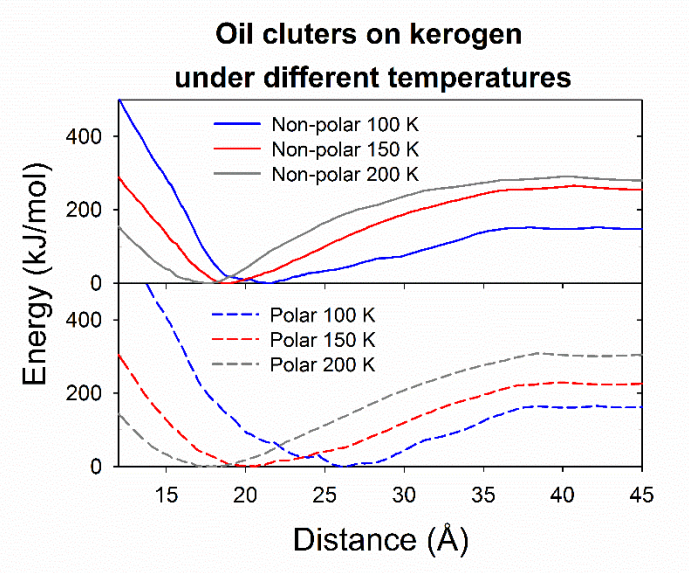

647

648 Fig S2. Free energy surfaces of 30-molecule oil drops interacting with kerogen surface under different
649 temperatures. According to the data point pattern on this chart, the correlation between desorption energy
650 and temperature can be formulated using the same equation below for both polar and non-polar oil. The
651 error bars are smaller than the symbol size.

652

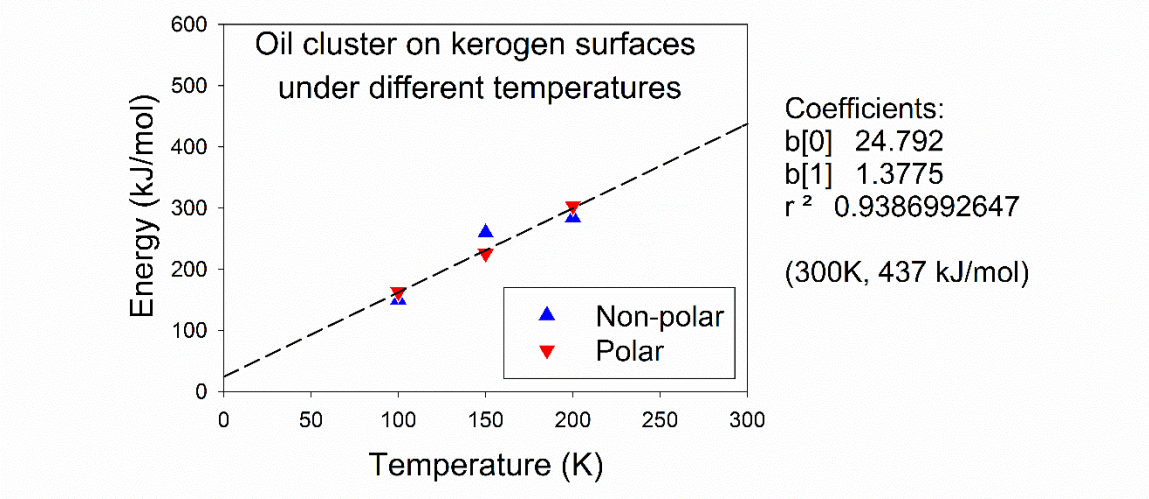

Fig S3. Desorption energies of 30-molecule oil drops on kerogen surfaces under different temperatures.

The non-polar and polar oil drops exhibit linear relationship between temperature and desorption energy (with a R-squared value of 0.9387). The non-polar and polar oil drops follow the same correlation between desorption energy (E_d in kJ/mol) and temperature (T in K):

$$E_d = 1.38 \cdot T + 24.8$$

The energy required for oil drop desorption from kerogen surface increases when the system temperature rises. As shown in Fig 9, a close examination on the interface of oil and surface reveals that molecules of oil drop are strongly attached to the kerogen surface. The same correlation of energy and temperature suggested that the intermolecular bonding between kerogen and oil are so strong that the effect of oil polarity is negligible during such interactions.

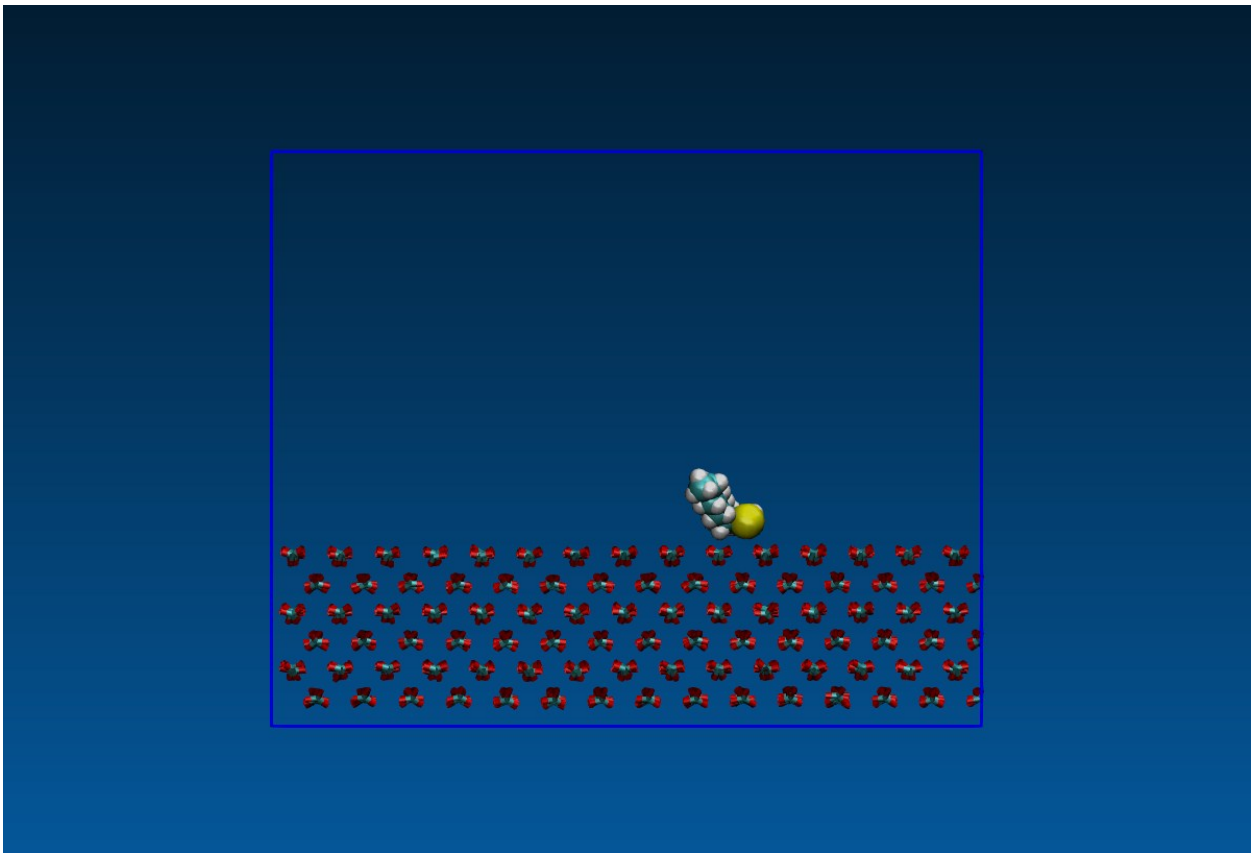

Fig S4. Snapshot of the simulation trajectory of calcite surface interaction with polar oil molecule in the absence of water.

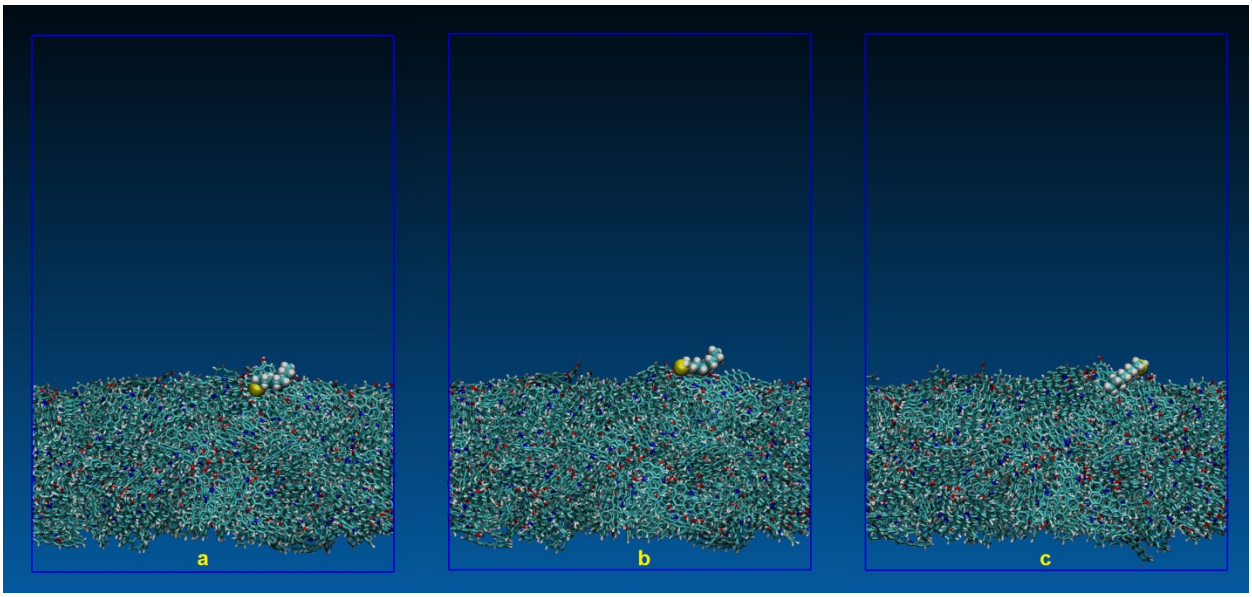

Fig S5. Snapshot of the simulation trajectory of kerogen surface interaction with polar oil molecule in the absence of water at different time step. (a) and (b) depict strong interactions between polar oil functional group –SH and kerogen functional groups –NH– and –OH, whereas (c) illustrates strong interactions between non-polar carbon chain of polar oil and non-polar benzene rings of kerogen.

677 Table S1. Desorption energies of oil drops on kerogen surface under different temperatures in the absence
678 of water.

Desorption energy in kJ/mol [error]		
Temperature	Non-polar	Polar
100 K	150.5 [2.5]	163 [3]
150 K	260 [5.5]	226 [3]
200 K	285 [5.5]	304 [5]

679